

Electrochemical Synthesis of TiO₂ Photocatalyst with Anodic Porous Alumina

Takanori Hattori, Takayoshi Fujino[†] and Seishiro Ito

Department of Applied Chemistry, Faculty of Science & Technology, Kinki University, 3-4-1 Kowakae, Higashiosaka, Osaka 577-8502, Japan.

(Received September 3, 2007 : Accepted November 5, 2007)

Abstract Aluminum was anodized in a H₂SO₄ solution, and titanium (IV) oxide (TiO₂) was electrodeposited into nanopores of anodic porous alumina in a mixed solution of TiOSO₄ and (COOH)₂. The photocatalytic activity of the prepared film was analyzed for photodegradation of methylene blue aqueous solution. Consequently, we found it was possible to electrodeposit TiO₂ onto anodic porous alumina, and synthesized it into the nanopores by hydrolysis of a titanium complex ion under AC 8-9 V when film thickness was about 15-20 μm. The photocatalytic activity of TiO₂-loaded anodic porous alumina (TiO₂/Al₂O₃) at an impressed voltage of 9 V was the highest in every condition, being about 12 times as high as sol-gel TiO₂ on anodic porous alumina. The results revealed that anodic porous alumina is effective as a substrate for photocatalytic film and that high-activity TiO₂ film can be prepared at low cost.

Key words TiO₂, Photocatalyst, Anodic porous alumina, Electrodeposition, Titanium complex ion.

1. Introduction

Photocatalysts generate electrons and positive holes by light energy, and it is possible to employ them to photolyze water,¹⁾ detoxify organic compounds and NO_x²⁻⁴⁾ and so on due to their possessing strong redox potential. TiO₂ in particular is a promising photocatalyst material that has often been studied because it has proved to be excellent in photocatalytic activity and resistance to photocorrosion.⁵⁻⁸⁾

The immobilization of photocatalyst to a substrate is indispensable when it comes to practical use, but cost and adhesion must be considered. Methods using an organic binder and a sol-gel method are the mainstream at present, but they present problems with cost, safety, and adhesion. In addition, photocatalytic activity is reduced because surface area becomes small through immobilization. Since photocatalytic activity is influenced by crystallinity, surface area, and impurities,⁹⁻¹³⁾ when photocatalytic film is immobilized, the selection of substrate is important.

Aluminum is widely used in building fields because it is cheap and light. However, since aluminum has low corrosion resistance, it is generally used as a surface finish, such as in anodizing, plating, and chemical conversion.

Anodized aluminum is just ideal material as a substrate of photocatalyst because it is porous and possesses a large surface area.

The aim in this report is to prepare an inexpensive and high-activity photocatalytic film by utilizing anodic porous alumina: an aluminum plate was anodized in a H₂SO₄ solution, and then TiO₂ was electrodeposited into nanopores by the same method as that used in electrolytic coloring. After that, the prepared film was sintered at 723 K. The photocatalytic activity of the prepared film was analyzed by photodegradation of the methylene blue (MB) aqueous solution.

2. Experimental procedures

An aluminum plate (purity: 99.85%, 30×50×0.4 mm) was pretreated by immersion in a NaOH aqueous solution, after which it was anodized by DC constant-current electrolysis under a current density of 2×10² A·m⁻² in a mixed solution of 50 mol·m⁻³ Al₂(SO₄)₃ and 1.5 kmol·m⁻³ H₂SO₄ for 30 min at 298 K.¹⁴⁻¹⁵⁾ A platinum plate (30×50×0.2 mm) was used as the counter electrode. Next, the TiO₂ was electrodeposited into the anodic porous alumina by AC constant-voltage electrolysis for electrolytic times of 1-10 min under impressed voltages of 6-15 V and 283 K in a mixed aqueous solution consisting of 50 mol·m⁻³ TiOSO₄ and 300

[†]Corresponding author

E-Mail : taka-f@apch.kindai.ac.jp (Takayoshi Fujino)

$\text{mol} \cdot \text{m}^{-3}$ $\text{H}_2\text{C}_2\text{O}_4$ dissolved by heating in water at 323 K, and then adjusted to pH 5 by an NH_4OH solution. The TiO_2 -loaded anodic porous alumina ($\text{TiO}_2/\text{Al}_2\text{O}_3$) was then sintered at 723 K.

Quantitative analysis of the TiO_2 was carried out by inductively coupled plasma (ICP) emission spectrometry, where the films were dissolved in heated conc. H_2SO_4 , followed by analysis of the resulting solution. The deposited TiO_2 was distinguished by X-ray diffraction (XRD) with $\text{CuK}\alpha$ radiation in the range of angles 20° - 90° because the peak of anatase-type TiO_2 can be detected with in this range. In addition, the prepared film was distinguished by $\text{MgK}\alpha$ excited X-ray photoelectron spectrometry (XPS). The $\text{TiO}_2/\text{Al}_2\text{O}_3$ was analyzed using thermal analysis equipment (TG/DTA). After being flaked and comminuted, the film was analyzed within the range of 298-1273 K (10 K/min) in an air. A micro-type platinum cell was used as the sample cell. The absorption spectrum of the film was measured by UV/vis absorption spectrometry within wavelength range of 250-500 nm, with absorbance defined as the logarithm of the intensity ratio of incident beam (I_0) and transmitted beam (I); $-\log(I/I_0)$. Deposition behavior of electrodeposited TiO_2 was confirmed by depth direction analysis and cross-sectional observation. The depth profile was examined using secondary ion mass spectroscopy (SIMS) under the conditions presented in Table 1.

The cross-sectional images were observed by trans-

Table 1. Analysis conditions of SIMS.

Primary beam	
Analysis mode	Depth
Ion species	O^{2+}
Acceleration voltage/kV	8
Intensity/nA	100
Secondary beam	
Polarity	Positive
Analysis area/mm	60
Electron gun	ON

Table 2. Working conditions on MB degradation

Test piece size/ mm^2	1500
Source of light	Black light ($\lambda_{\text{max}} = 254 \text{ nm}$, $3 \text{ W}\ddot{\text{A}}\text{Em}^{-2}$)
Volume of methylene blue/ m^3	4×10^{-5}
UV illumination time/h	2
Analysis wavelength/nm	663

mission electron microscopy (TEM) under 300 kV of acceleration voltage. The photocatalytic activity was analyzed for the photocatalytic reduction of the MB. The MB solution was set to 10 ppm and placed into a 4×10^{-5} m^3 vessel with samples and the vessel were illuminated with UV light from a black light during 2 h. Analysis was carried out under the conditions shown in Table 2, and then absorbance was determined using a UV/vis spectrophotometer at a wavelength of 663 nm.

3. Results and Discussion

3.1 State analysis of electrolytic solution

Fig. 1 shows the result that confirmed the state of titanium ions in the electrolytic solution by conductometric titration. The titrant was $\text{H}_2\text{C}_2\text{O}_4$, and the sample solution was set to 50 mol m^{-3} TiOSO_4 (eq.-i). The molar ratio of titanium to $\text{H}_2\text{C}_2\text{O}_4$ was 1 : 1 because endpoint appeared when $\text{H}_2\text{C}_2\text{O}_4$ was titrated to about 50 mol m^{-3} . Thus, the TiOC_2O_4 complex was formed in the solution (eq.-ii).

The solution's pH didn't change to the end point but had begun to decrease after that. H^+ concentration therefore didn't change before and behind the end point.

Chemical equation in the solution based on results of them is as follows:

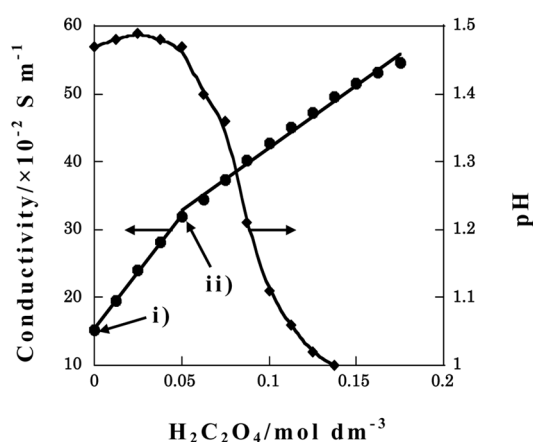
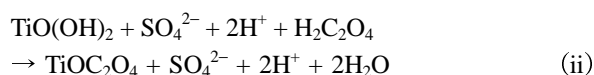
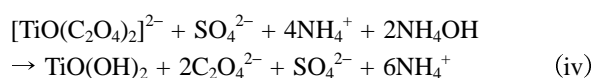
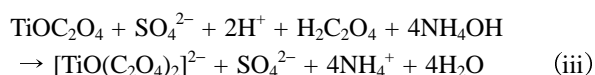


Fig. 1. Conductometric titration and pH change curves of TiOSO_4 solution using $\text{H}_2\text{C}_2\text{O}_4$ as titrant. Titrant: $\text{H}_2\text{C}_2\text{O}_4$; Sample solution: 50 mol m^{-3} TiOSO_4 .

Fig. 2 shows relationships between conductivity and pH of electrolytic solution and the chemical equation considered from it is indicated in the following. Eq.-iii shows addition of NH₃ aq. to the solution of eq.-ii. The conductivity was increased when the solution's pH was more than 3 because TiOC₂O₄ complex changed [TiO(C₂O₄)₂]²⁻ complex ion by configuration of C₂O₄²⁻.

On the other hand the inclination of the curve decreases in iii to iv. This is because TiO(OH)₂ formed by hydrolyzation of [TiO(C₂O₄)₂]²⁻ anion.



3.2 Electrodeposition behavior of TiO₂

Fig. 3 shows the depth profile of TiO₂/Al₂O₃. The elements of being measured are ⁴⁸Ti and ⁴⁶Ti, and for reference, anodic porous alumina without TiO₂ was analyzed. Film thickness of the TiO₂/Al₂O₃ and anodic porous alumina was set to 2 μm. The ⁴⁶Ti and ⁴⁸Ti exhibited different behavior in reference sample, but in TiO₂/Al₂O₃ they behaved identically. The SIMS results, therefore, proved that TiO₂ was electrodeposited into the anodic porous alumina.

3.3 I-E curve in TiO₂ electrodeposition

Fig. 4 shows the I-E curve when electrodepositing TiO₂ in a mixed solution of TiOSO₄ and H₂C₂O₄. Current density was measured using a multimeter for an

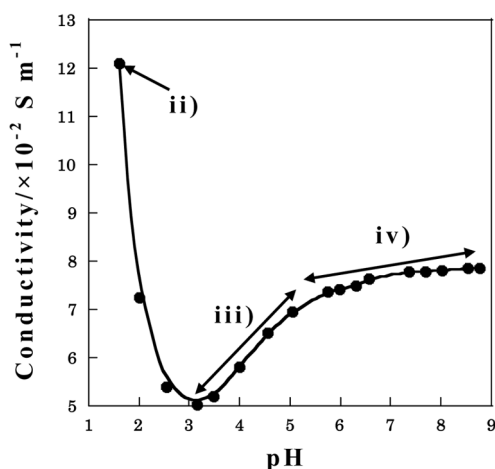


Fig. 2. pH vs conductivity curves of H₂C₂O₄ and TiOSO₄ mixture solution using conc. NH₄ aqueous solution as titrant.

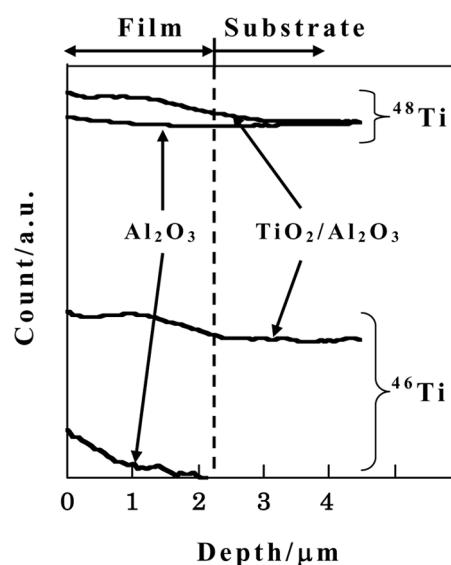


Fig. 3. Depth profile of TiO₂/Al₂O₃ and anodic porous alumina by SIMS.

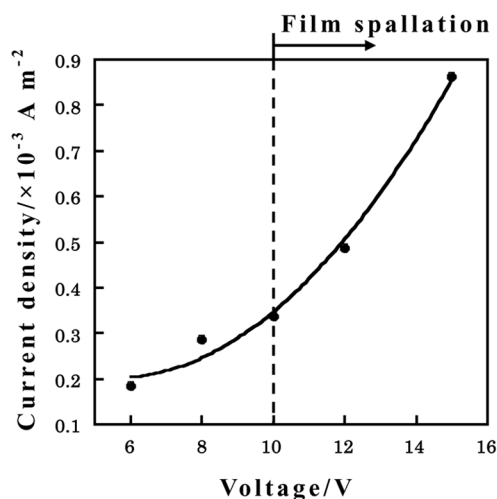


Fig. 4. I-E curve when electrodepositing TiO₂ in anodic porous alumina of film thickness 15 μm.

electrolytic time of 5 min under impressed voltages of 6–15 V. Current density increased as an exponential function with voltage, and it was confirmed that the anodic porous alumina flaked off from the Al substrate when the impressed exceeded 10 V. This occurred because the increase of current density generated remarkable quantities of hydrogen and that lifted the film from the substrate.

The appropriate voltage, therefore, was 8–9 V when electrolyzing in this solution. However the appropriate voltage is considered to change due to anodic porous alumina because breakthrough voltage of the barrier layer depends on kind of the film.

3.4 Amount of TiO₂ inside nanopores

Fig. 5 shows the amount of electrodeposited TiO₂ when changing voltage. It is clear that when the voltage was changed, the amount of TiO₂ increased proportionally with voltage to 9 V, but began to decrease when voltage exceeded 10 V. In other words, anodic porous alumina and/or deposited TiO₂ became flaked with impression of more than 10 V.

The temporal amount change of TiO₂ at AC 9 V is shown in Fig. 6. The amount of TiO₂ increased in proportion with time as the voltage changed, and began to decrease when electrolytic time exceeded 10 min. The electrodeposited amount of TiO₂ was limited to about $2.5 \times 10^{-5} \text{ kg} \cdot \text{m}^{-2}$ when the thickness of the porous alumina was 15 μm .

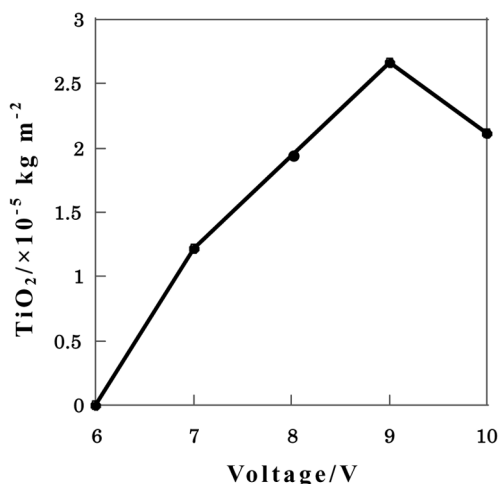


Fig. 5. Amount of TiO₂ in anodic porous alumina when changing voltage in electrolytic time for 5 min.

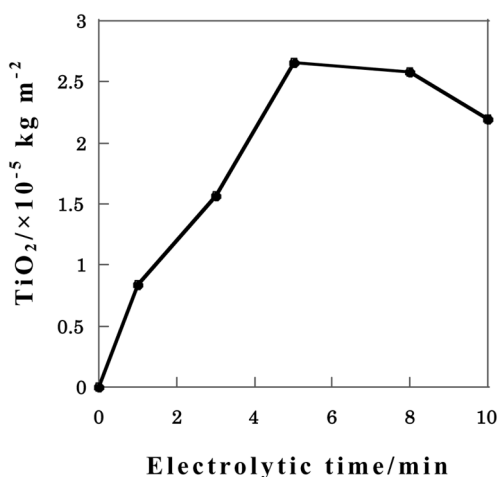


Fig. 6. Amount of TiO₂ in anodic porous alumina when changing electrolytic time in impressing voltage under AC 9 V.

3.5 Characterization of TiO₂/Al₂O₃

Flaked and comminuted TiO₂/Al₂O₃, and as a reference anodic porous alumina without TiO₂ and amorphous TiO₂ were analyzed using TG-DTA measurement, and the respective peaks were denoted with A, B, C, D and E. The measurement results are shown in Fig. 7. The amorphous TiO₂ particles were synthesized by hydrolyzation of the electrolytic solution with NH₄OH, and then analyzed after drying. Peak A was confirmed in all samples. This is the endothermic peak at approximately 380 K in a DTA spectrum that is considered to be due to removal of adsorbed water. Peaks B and C were peaks of TiO₂ because they were not confirmed in the anodic porous alumina but appeared in the TiO₂ and the TiO₂/Al₂O₃. First, peak B was the endothermic peak at about 580 K representing the elimination of water from TiO₂. Next, peak C at approximately 600 K was considered the peak denoting the phase transition to anatase-type TiO₂ because it was the exothermic peak. Peaks D and E appeared only in the anodic porous alumina and TiO₂/Al₂O₃ these peaks are therefore considered to depend on the anodic porous alumina. Peak D at around 900 K was considered to denote the wide endothermic reaction according to the dehydration reaction from the anodic

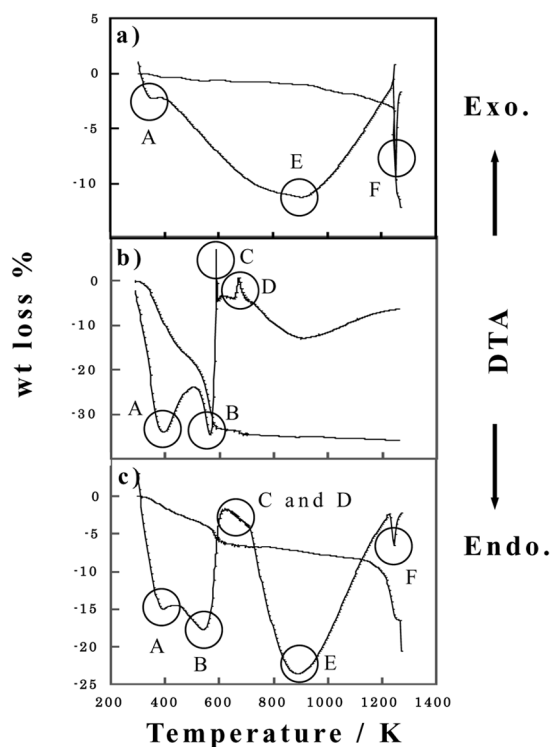


Fig. 7. TG/DTA curves of a) anodic porous alumina; b) amorphous TiO₂ · H₂O and c) TiO₂/Al₂O₃.

porous alumina, and peak E at 1300 K represented the changing of amorphous Al₂O₃ to α -Al₂O₃. In the TG result for TiO₂ particles (Fig. 6-b), this is regarded as the halting of the dehydration reaction in TiO₂. This product was proved to be TiO₂ · H₂O because a decrease of about 18wt% was detected at temperatures of about 580 K.

Fig. 8 shows the XRD patterns of TiO₂. The anodic porous alumina was electrolyzed by AC 30 V in a mixed solution of TiOSO₄ and H₂C₂O₄, and then settled TiO₂ particles were analyzed by powder XRD, which revealed that morphology of electrodeposited product was amorphous. However, the product crystallized to anatase-type TiO₂ upon heating.

Fig. 9 shows the XPS of the product deposited into pores. The spectra when insulating material was analyzed

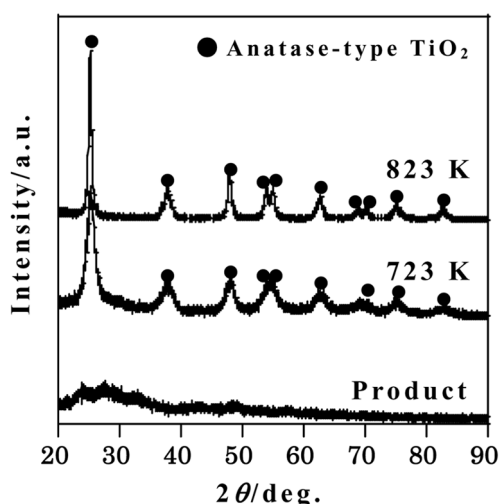
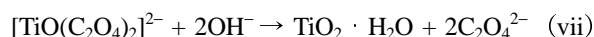
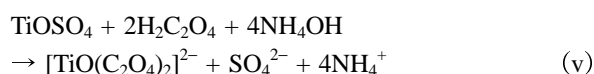


Fig. 8. XRD patterns of precipitated products after electrolysis.

and had to be calibrated with the standard sample. Generally, the calibration is often carried out using the C 1s (284.6 eV) spectrum of impurity carbon that exists on all samples. The Ti 2p spectrum (Fig. 9-a) shows two peaks located at 458.5 eV and 464.2 eV, respectively; only the peak that indicates TiO₂ was observed in the Ti 2p spectrum as well as the XRD results. On the other hand, The O 1s spectrum is shown in Fig. 9-b. The spectrum includes two peaks located at 529.9 eV and 531.8 eV that respectively indicate TiO₂ and anodic porous alumina (Al₂O₃) respectively.

Thus, from the results of TG/DTA, XRD and XPS, the product electrodeposited into nanopores was amorphous TiO₂ · H₂O, which then crystallized to anatase-type TiO₂ by heating at around 600 K.

The electrodepositing process of TiO₂ in this method is different from metal deposition in conventional electrolytically colored anodic oxide coating, depending on hydrolyzation and not on electrochemical reduction. The considered TiO₂ electrodeposition mechanism based on results of the conductometric titration and characterization is as follows:



First, Eq.-v is the equation for the electrolytic solution explained already in sect. 3.1. Next, water electrolyzed to hydrogen and the hydrate anion by impression of the AC

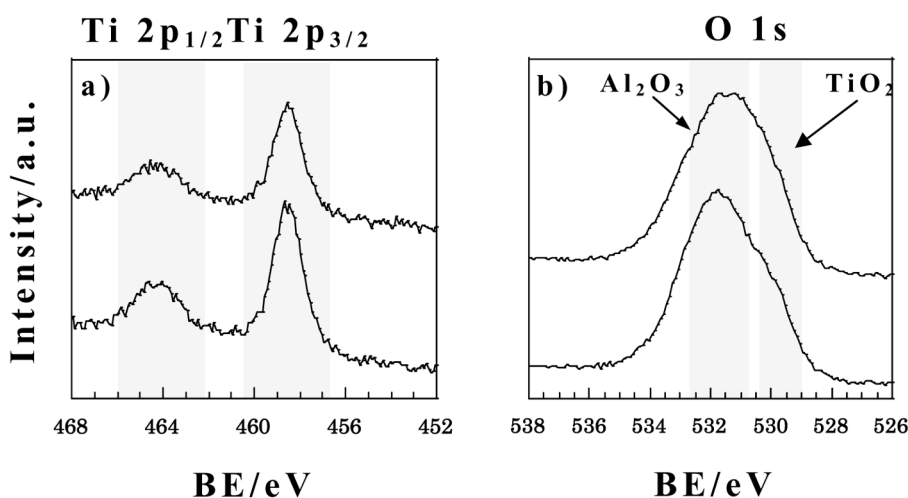


Fig. 9. XPS of electrodeposited products: a) crystallized product at 723 K (TiO₂); b) electrodeposited product.

voltage at more than 8 V (Eq.-vi). Thus, the pH of the interface was increased, and TiO₂ was deposited by hydrolysis of the [TiO(C₂O₄)₂]²⁻ ion (Eq.-vii).

The UV/vis absorption spectrum of sintered TiO₂/Al₂O₃ at 723 K and reference samples [anodic porous alumina, the marketed anatase-type TiO₂ (average diameter: 150 nm), and the marketed rutile-type TiO₂ (average diameter: 300 nm)] are shown in Fig. 10. The red-shift in the absorption region depends on deposited TiO₂ because the absorption edge of TiO₂/Al₂O₃ was around 340 nm; the absorption wavelength was clearly greater than that of the oxidation film. On the other hand, the absorption edge was shorter than that of the bulk TiO₂ because the blue shift is caused by the quantum size effect, which has already been explained.¹⁶⁻¹⁹ The size of TiO₂ is sufficiently small because it was immobilized into nanopores (pore diameter: approx. 10 nm) of the anodic porous alumina, so it is possible that the quantum size effect is manifested in TiO₂/Al₂O₃.²⁰⁻²²

3.6 Photocatalytic activity of the TiO₂/Al₂O₃

Fig. 11 illustrates the temporal concentration changes of MB in photocatalytic reactions, and the rate constant of MB degradation is shown in Table 3. The rate constant was calculated using the following equation.

Rate const. $k = \ln(C/C_0) \cdot t^{-1}$ (C = MB concentration, C_0 = MB initial concentration, t = UV illumination time)

The photocatalytic activity was evaluated from the logarithm of the concentration ratio of MB, which was

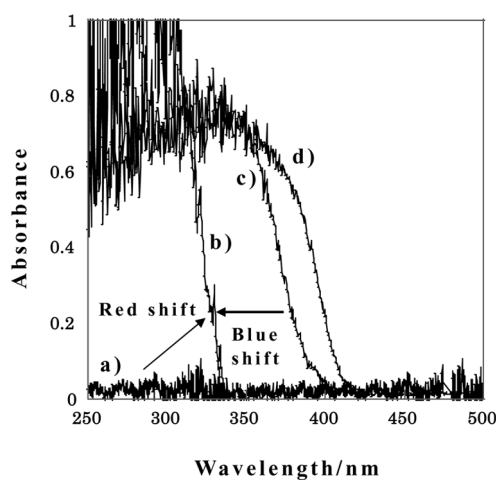


Fig. 10. UV/vis absorption spectra of a) marketed rutile-type TiO₂ (average diameter:300 nm); b) marketed anatase-type TiO₂ (average diameter:150 nm); c) TiO₂/Al₂O₃ and d) anodic porous alumina.

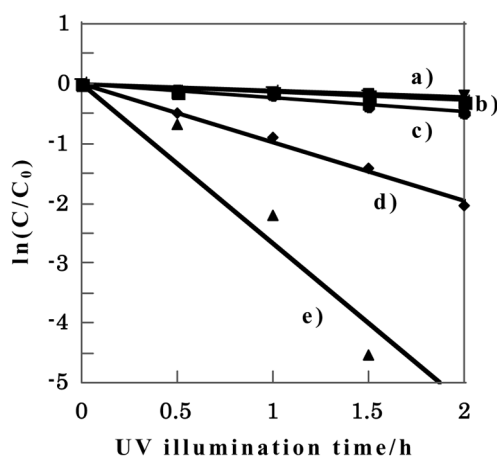


Fig. 11. Time course of concentration of methylene blue under black light illumination ($\lambda = 254$ nm) for 2 hour: a) Blank; b) AC 6 V-TiO₂/Al₂O₃; c) sol-gel TiO₂ on anodic porous alumina; d) AC 8 V-TiO₂/Al₂O₃ and e)AC 9 V-TiO₂/Al₂O₃.

Table 3. Rate constant of MB degradation

Sample	k/h^{-1}
Blank	0.113
Sol-gel TiO ₂	0.249
AC 6 V	0.131
AC 8 V	0.940
AC 9 V	3.016

proportional in terms of ultraviolet ray illumination time and decreased in a straight line. The results confirmed the clear differences in absorbance changes: photocatalytic activity was confirmed to manifest when impressed voltage was more than 8 V, and it was higher than TiO₂ onto anodic porous alumina produced by the sol-gel

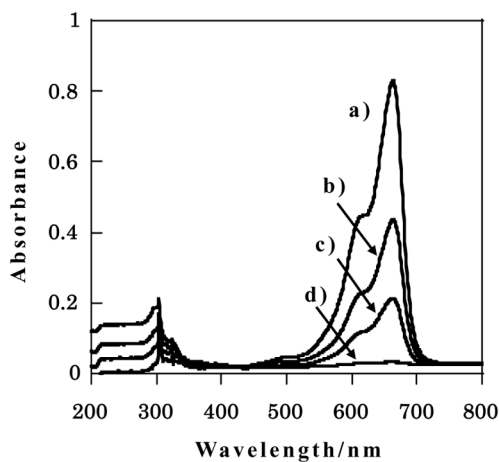


Fig. 12. Absorbance change of methylene blue for time course in 9 V- TiO₂/Al₂O₃: a) 0 hour; b) 0.5 hour c) 1 hour and d) 1.5 hour.

method. This is because TiO₂ was electrodeposited uniformly along the walls of pores and its large surface area was utilized effectively. The activity of 9 V-TiO₂/Al₂O₃ in particular was the highest under every condition because most TiO₂ was loaded into the anodic porous alumina, and the 10 ppm MB was perfectly decolorized by 9 V-TiO₂/Al₂O₃ at about 1.5 hours as shown in Fig. 12. However, TiO₂ deposited under AC 6 V almost did not decompose the MB. The rate constant of degradation was almost same as a blank because TiO₂ was not electrodeposited when impressing AC 6 V at all, as already indicated by ICP analysis.

3.7 Cross-sectional images of films

Fig. 13 shows the cross-sectional micrographs of the TiO₂/Al₂O₃ films by TEM. Nanopores formed vertical

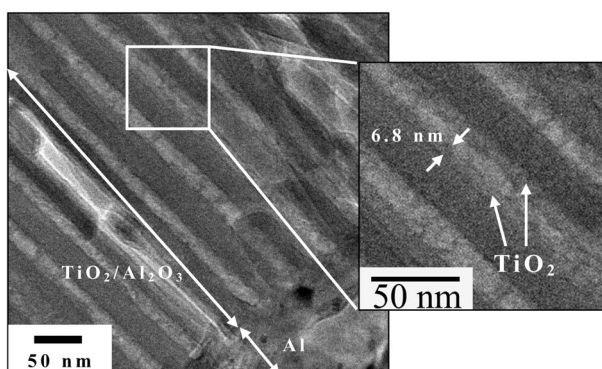


Fig. 13. Cross-sectional image of TiO₂/Al₂O₃ film by TEM

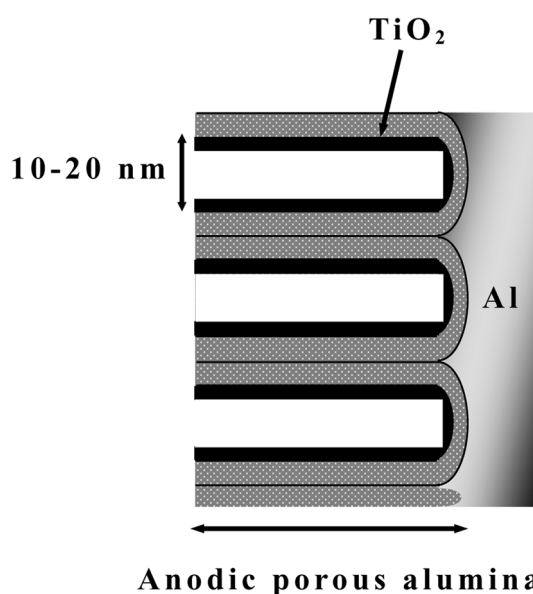


Fig. 14. Scheme of TiO₂/Al₂O₃ expected from the SIMS result.

lines lengthwise to an aluminum substrate from the interface, and diameter of the pores was about 10-20 nm. TiO₂ nanoparticles of smaller than 10 nm of diameter were electrodeposited on wall of anodic porous alumina. Also, Fig. 14 shows the cross-sectional scheme of TiO₂/Al₂O₃. The SIMS and TEM results concluded the TiO₂ was electrodeposited uniformly along the walls of the pores.

4. Conclusion

It was possible to electrodeposit TiO₂ into anodic porous alumina in a mixed solution of TiOSO₄ and H₂C₂O₄. It was synthesized into nanopores by hydrolysis of a titanium complex ion ([TiO(C₂O₄)₂]²⁻) under AC 8-9 V when film thickness of anodic porous alumina was about 15-20 μm. TiO₂/Al₂O₃ manifested high photocatalytic activity, which in particular at an impressed voltage of 9 V was about 12 times as high as sol-gel TiO₂ on anodic porous alumina. This is because TiO₂ was electrodeposited uniformly along the walls of pores and that its large surface area was utilized effectively.

Therefore, anodic porous alumina is effective as a substrate for photocatalytic film and high-activity TiO₂ since it is inexpensive to produce, making it attractive to industry.

Acknowledgements

This work was supported by funding from the Ministry of Education, Culture, Sports, Science and Technology private school grant. The authors thank them for their immense assistance in the development of anodic alumina and its applicability.

References

1. A. Fujishima and K. Honda, *Nature*, **238**[5358] (1972) 37-38
2. T. Inoue, A. Fujishima, S. Konishi and K. Honda, *Nature*, **277** (1979) 637-638.
3. N. Negishi, K. Takeuchi and T. Ibusuki, *Applied surface science*, **121/122** (1997) 417-420.
4. Y. Komazaki, H. Shimizu and S. Tanaka, *Atmospheric Environment*, **33**[27] (1999) 4363-4371.
5. A. Ishizaki, *Hyoumen gijutsu*, **50** (1999) 251-255. (in Japanese)
6. Y. Yamaguchi, *Hyoumen gijutsu*, **50** (1999) 256-259. (in Japanese)
7. H. Takeuchi, *Hyoumen gijutsu*, **50** (1999) 260-264. (in Japanese)
8. M. Anpo, T. Morizane, T. Inui, K. Kato, E. Nomura, and

- H. Taoda, in *Saishin hikarishokubai gijutsu* (NTS Co.Ltd, 2000), p. 11-12. (in Japanese)
9. Z. S. Wang, C. H. Huang, Y. Y. Huang, and B. W. Zhang, *Solar Energy Materials and Solar Cells*, **71**[2] (2002) 261-271.
10. K. Hara, T. Horiguchi, T. Kinoshita, K. Sayama, and H. Arakawa, *Solar Energy Materials and Solar Cells*, **70**[2] (2001) 151-161.
11. R. N. Viswanath and A. Chandra, *J. Physics and Chemistry of Solids*, **62**[11] (2001) 1991-1998.
12. R. Fretwell and P. Douglas, *J. Photochemistry and Photobiology A*, **143**[2-3] (2001) 229-240.
13. Y. Guo, M. Sakurai, H. Kameyama, A. Matsuyama, and Y. Kudoh, *J. of The Surface Finishing Society of Japan*, **55** (2004) 366-372. (in Japanese)
14. T. Fujino and T. Nara, *Kinki Aruminiumu Hyomen Shori Kenkyukai Kaishi*, **216** (2002) 1-4. (in Japanese)
15. T. Fujino and T. Nara, *Keikinzo*, **53**[10] (2003) 410-415. (in Japanese)
16. M. Anpo, N. Aikawa, Y. Kubokawa, M. Che, C. Louis, E. Giamello, *J. Physical Chemistry*, **89** (1985) 5017.
17. Z. Hua, J. Shi, L. Zhang, M. Ruan, J. Yan, *Advanced Materials*, **14**[11] (2002) 830-833
18. J. J. Schneider, N. Czap, J. Hagen, J. Engstler, J. Enslin, L. Jos De Jongh, M. Wark, G. Grubert, G. L. Hornyak, R. Zannoni, *Chemistry-A European Journal*, **6**[23] (2000) 4305-4321
19. H. Yamashita, S. Kawasaki, Y. I. Chihashi, M. Harada, M. Takeuchi, M. Anpo, G. Stewart, M. A. Fox, C. Louis, M. Che, *J. Physical Chemistry B*, **102**[30] (1998) 5870-5875
20. Li, Jinhong; Shi, Xiaoying; Wang, Lijuan; Liu, Fei, *Journal of Colloid and Interface Science*, **315**[1] (2007) 230-236.
21. T. Maiyalagan, B. Viswanathan, U. V. Varadaraju, *Bulletin of Materials Science*, **29**[7] (2006) 705-708.
22. K. Honda, T. Yoshikawa, *Bunseki Kagaku*, **56**[1] (2007), 51-54. (in Japanese)